metals

MDPI

Article

Experimental Investigation of Phase Equilibria in the Co-Re-Ta Ternary System

Xingjun Liu [1,2], Dan Wu [1], Jinbin Zhang [1], Mujin Yang [1], Jiahua Zhu [1], Lingling Li [1], Yuechao Chen [1], Shuiyuan Yang [1], Jiajia Han [1], Yong Lu [1] and Cuiping Wang [1,*]

1 College of Materials and Fujian Provincial Key Laboratory of Materials Genome, Xiamen University, Xiamen 361005, China; lxj@xmu.edu.cn (X.L.); wudan225@163.com (D.W.); jbzhang@xmu.edu.cn (Jin.Z.); mujinguagua123@gmail.com (M.Y.); zhujiahua@stu.xmu.edu.cn (Jia.Z.); xmulee@foxmail.com (L.L.); cycofxmu@foxmail.com (Y.C.); yangshuiyuan@xmu.edu.cn (S.Y.); jiajiahan@xmu.edu.cn (J.H.); luyong@xmu.edu.cn (Y.L.)

2 State Key Laboratory of Advanced Welding and Joining, Harbin Institute of Technology, Shenzhen 518005, China

* Correspondence: wangcp@xmu.edu.cn; Tel.: +86-592-218-0606; Fax: +86-592-218-7966

Received: 20 October 2018; Accepted: 31 October 2018; Published: 6 November 2018

Abstract: In this study, the isothermal sections of the Co-Re-Ta ternary system at 1100, 1200, and 1300 °C have been experimentally investigated by means of electron probe microanalysis and X-ray diffraction. The results indicated the following: (1) The solid solubilities of the λ_3, (εCo, Re), χ-Re_7Ta_3, and bcc-(Ta) phases were large and changed very little from 1100 to 1300 °C; (2) more interestingly, the λ_2 phase, with a very limited solubility of Re, was surrounded by the λ_3 phase; (3) the solubility of Re for the μ-Co_6Ta_7 phase increased slowly from 1100 to 1300 °C. These experimental results will be useful for Co-based high-temperature alloys, especially as a supplement for thermodynamic databases.

Keywords: Co-Re-Ta; phase diagram; high-temperature alloys; electron probe microanalysis

1. Introduction

It was first found by Sato et al. [1] that Co-based superalloys were strengthened by a stable ternary compound, γ′ Co_3(Al, W), with the $L1_2$ structure. Subsequently, the Co-based superalloys have been regarded as one of the promising high-temperature materials that exhibit better high-temperature strength than the conventional Ni-based superalloys [1]. To further improve high-temperature properties of Co-based superalloys, some refractory alloying elements, such as Re, Ta, W, and Mo, have been added to materials, which can improve high-temperature mechanical properties, creep properties, corrosion, and oxidation resistance [2–11]. Re does not randomly distribute in the alloy; it hinders dislocation movement by forming tiny clusters which act as obstacles during creep tests [2–5]. Thus, the addition of Re can effectively enhance the creep properties of superalloys. Meanwhile, as Re content increases, it refines the morphology and enhances the content of the alloy compound for Co-based superalloys [6]. Doping of Ta can maintain good microstructural stability and improve oxidation resistance [7,8]. The amount of Re and Ta additions is strictly restricted because excessive additions will cause the brittle and detrimental TCP (topologically close packed) phases to form at high stresses and temperatures [9–11]. Therefore, the knowledge of phase equilibria in the Co-Re-Ta ternary system is essential, which will provide significant basic data for the design of Co-based superalloys. However, there is no information on the experimental investigation of and thermodynamic data for the Co-Re-Ta ternary system. It is necessary to investigate the phase equilibria of the Co-Re-Ta ternary system.

The three binary systems, Co-Re, Re-Ta, and Co-Ta, that constitute the Co-Re-Ta ternary system are shown in Figure 1.

Elliott [12] has published the results for the Co-Re binary system. Later, Predel [13] reported the results for the Co-Re binary system based on experimental data. Recently, Liu et al. [14] and Guo et al. [15] estimated the Co-Re system and their findings were consistent with the experimental data. The newly assessed Co-Re phase diagram by Guo et al. [15] was applied in this work. The Co-Re system [15] is simple because there are two solid phases of (αCo) and (εCo, Re) and no intermediate phases. The (εCo, Re) phase has a wide homogeneity range.

The Re-Ta binary system was first studied by Greenfield and Beck [16]. They investigated alloys with Ta contents between 25 and 52 at. % and reported the composition range of the σ and χ phases. Cui and Jin [17] treated the σ phase as a stoichiometric phase and thermodynamically assessed the Re-Ta system. Afterwards, Liu and Chang [18] also evaluated the thermodynamic description of the Re-Ta system. Recently, Guo et al. [15] estimated the Re-Ta phase diagram with the latest thermodynamic description for pure Re, and this Re-Ta binary system was used in the paper. The two intermediate phases of χ-Re_7Ta_3 and σ-Re_3Ta_2 exist in the Re-Ta binary system [15]. The σ-Re_3Ta_2 phase forms from the peritectic reaction of liquid + χ-Re_7Ta_3 ↔ σ-Re_3Ta_2. The melting point of the χ-Re_7Ta_3 phase is about 2832 °C.

The Co-Ta binary system has been investigated by many researchers [19–24]. Itoh et al. [19] investigated the homogeneity ranges, crystal structures, and magnetic properties of the three Laves phases in the Co-Ta system. Okamoto [20] assessed the Co-Ta phase diagram and treated C14 as a line compound. Liu and Chang [21] thermodynamically assessed the Co-Ta binary system. Shinagawa et al. [24] studied the Co-Ta binary system and revised the λ_1 phase as an intermetallic compound with a narrow composition range, and the phase diagram [24] was adopted in this work. There are three Laves phases of λ_1 (C14), λ_2 (C15), and λ_3 (C36), each with different polytypes. The other intermediate phases of $CoTa_2$, μ-Co_6Ta_7, and Co_7Ta_2, and solution phases of bcc-(Ta), (εCo), and (αCo) also exist in the Co-Ta binary system. The λ_1 and λ_3 phases are obtained from peritectic reactions of liquid + λ_2 ↔ λ_1 and liquid + λ_2 ↔ λ_3, respectively. The λ_1 phase exists at ~1293–1587 °C and the λ_3 phase exists at ~947–1456 °C. The Co_7Ta_2 phase with the $BaPb_3$ [23] crystal structure is obtained from a peritectoid reaction: (αCo) + λ_3 ↔ Co_7Ta_2. The information for the stable solid phases and their crystal structures in the three binary systems is listed in Table 1.

The temperatures of 1100, 1200, and 1300 °C were selected because the Co-based superalloys are widely used in high-temperature areas such as aircraft engines and turbine blades. Thus, it is more meaningful to investigate the phase equilibria at high temperatures. The present work aimed to experimentally investigate the phase equilibria of the Co-Re-Ta ternary system at 1100, 1200, and 1300 °C using electron probe microanalysis and X-ray diffraction techniques in order to understand the microstructures of the Co-Re-Ta ternary system and provide useful information for the development of Co-based high-temperature alloys.

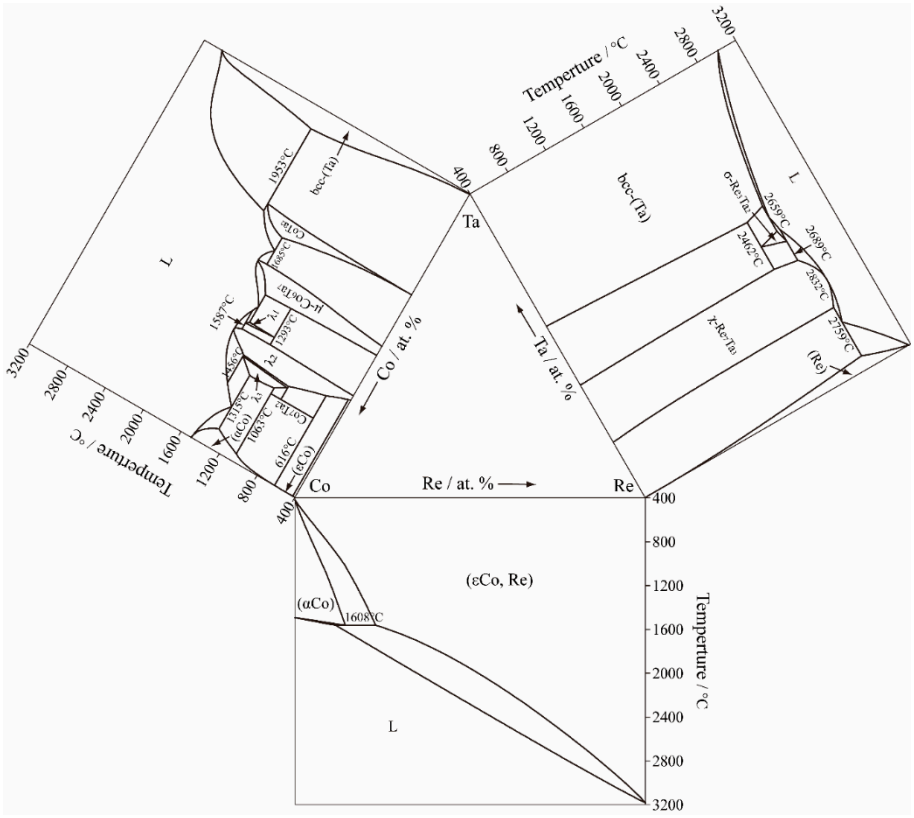

Figure 1. Binary phase diagrams constituting the Co-Re-Ta ternary system [15,24].

Table 1. Crystal structures of each phase in the Co-Re-Ta ternary system [15,23,24].

System	Phase	Pearson Symbol	Space Group	Prototype	Structure Type	References
Re-Ta	(Re)	*hP2*	*P6$_3$/mmc*	Mg	*A3*	[15]
	χ-Re_7Ta_3	*cI58*	*I-43m*	αMn	*A12*	[15]
	σ-Re_3Ta_2	*tP30*	*P4$_2$/mnm*	σCrFe	*D8$_b$*	[15]
	bcc-(Ta)	*cI2*	*Im-3m*	W	*A2*	[15]
Co-Re	(αCo)	*cF4*	*Fm-3m*	Cu	*A1*	[15]
	(εCo, Re)	*hP2*	*P6$_3$/mmc*	Mg	*A3*	[15]
Co-Ta	(αCo)	*cF4*	*Fm-3m*	Cu	*A1*	[24]
	(εCo)	*hP2*	*P6$_3$/mmc*	Mg	*A3*	[24]
	λ_3-Co_2Ta	*hP24*	*P6$_3$/mmc*	Ni_2Mg	*C36*	[24]
	λ_2-Co_2Ta	*cF24*	*Fd-3m*	Cu_2Mg	*C15*	[24]
	λ_1-Co_2Ta	*hP12*	*P6$_3$/mmc*	Zn_2Mg	*C14*	[24]
	μ-Co_6Ta_7	*hR13*	*R-3m*	Fe_7W_6	*D8$_b$*	[24]
	$CoTa_2$	*tI12*	*I4/mcm*	Al_2Cu	*C16*	[24]
	bcc-(Ta)	*cI2*	*Im-3m*	W	*A2*	[24]
	Co_7Ta_2	*hR36*	*R-3m*	$BaPb_3$ [23]	-	[23,24]

2. Experimental Procedure

High-purity rhenium (99.9 wt %), tantalum (99.9 wt %), and cobalt (99.9 wt %) were used as raw materials. The required weights of the elements (with a total weight of about 20 g) were measured with a semi-micro analytical balance with an accuracy of at least 0.5 mg. During the whole sample preparation procedure, the mass loss was usually less than 1%. Therefore, the mass loss was assumed to make no significant effect on the sample composition.

All the bulk alloys were prepared in the form of atomic ratios (at. %). The bulk alloys with nominal compositions were melted by arc-melting in an argon atmosphere using a non-consumable tungsten electrode on a water-cooled plate. Titanium was used as a getter material. The buttons were re-melted at least five times to ensure that the ingots were homogeneous.

Afterwards, the specimens were cut into small pieces by a wire-cutting machine for heat treatment. The samples were cleaned by an ultrasonic cleaner and then encapsulated in quartz ampoules which were evacuated and flushed several times with purified argon. Heat treatments were performed at 1100, 1200, and 1300 °C, respectively. The time of the heat treatments ranged from 15 days to 65 days to reach phase equilibria based on the different temperatures and compositions of the samples. The samples containing over 20 at. % Re were heat-treated for a relatively long time. Subsequently, the specimens were quenched, mounted, grinded, and polished.

The microstructural observation and equilibrium composition analysis of specimens was characterized by electron probe microanalysis (EPMA) (JXA-8100R, JEOL, Tokyo, Japan). Pure elements were used as standards and the measurements were carried out at a voltage of 20 kV and a current of 1.0×10^{-8} A. To identify the crystal structures, powder X-ray diffraction (XRD) measurements were performed on a Philips Panalytical X-pert diffractometer (Bruker Daltonic Inc., Billerica, MA, USA) with Cu Kα radiation at 40 kV and 40 mA. The scanning range of 2θ was from 20° to 90° at a step size of 0.0167°.

3. Results and Discussion

3.1. Microstructure

The typical back-scattered electron (BSE) images of ternary Co-Re-Ta alloys annealed at 1100, 1200, or 1300 °C for different times are shown in Figure 2; there are three-phase equilibrium microstructures shown in Figure 2a–d and two-phase equilibrium microstructures shown in Figure 2e–j. The corresponding results of the XRD are presented in Figure 3.

For the $Co_{74}Re_{16}Ta_{10}$ alloy, the light grey phase ((εCo, Re)), dark grey phase (λ_3), and black phase ((αCo)) were observed after annealing at 1100 °C for 50 days, as shown in Figure 2a. Figure 2b shows the three-phase equilibrium of the μ-Co_6Ta_7 phase, λ_3 phase, and bcc-(Ta) phase in the 1200 °C/35 days-annealed $Co_{44}Re_{14}Ta_{42}$ alloy. The white phase was bcc-(Ta), the light grey phase was μ-Co_6Ta_7, and the dark grey phase was λ_3. Figure 3a shows that the corresponding XRD pattern, and the μ-Co_6Ta_7 phase, λ_3 phase, and bcc-(Ta) phase were clearly distinguished by the different symbols. The $Co_{31}Re_{35}Ta_{34}$ alloy annealed at 1300 °C for 25 days contained the three phases of χ-Re_7Ta_3 (light grey), bcc-(Ta) (dark grey), and λ_3 (black), which are shown in Figure 2c. The λ_3 phase was the matrix while the bcc-(Ta) phase was on the edge of the χ-Re_7Ta_3 phase. XRD identification, as shown in Figure 3b, confirmed the existence of the three phases of χ-Re_7Ta_3, bcc-(Ta), and λ_3. Figure 2d shows the BSE image of the $Co_{45}Re_{30}Ta_{25}$ alloy annealed at 1300 °C for 25 days. There were three phases of λ_3, χ-Re_7Ta_3, and (εCo, Re) existing in an equilibrium. Figure 2e shows a two-phase microstructure constituted by a white (εCo, Re) phase and a black λ_3 phase in the $Co_{54}Re_{25}Ta_{21}$ alloy quenched from 1100 °C. The two-phase equilibrium of bcc-(Ta) and $CoTa_2$ was identified in the annealed $Co_{22}Re_5Ta_{73}$ alloy (1100 °C/50 days), as shown in Figure 2f. In the $Co_{58}Re_3Ta_{39}$ alloy annealed at 1200 °C for 35 days, the white μ-Co_6Ta_7 phase and the dark grey λ_3 phase were observed in Figure 2g while their crystal structure was confirmed by the XRD pattern in Figure 3c. Figure 2h shows the BSE image of the bcc-(Ta) phase and the μ-Co_6Ta_7 phase in the $Co_{25}Re_{20}Ta_{55}$ alloy annealed at 1200 °C for 50 days. The white bcc-(Ta) phase was homogeneously distributed in the grey μ-Co_6Ta_7 phase. Figure 2i shows that the two phases of λ_3 and (αCo) were found in the $Co_{80}Re_{11}Ta_9$ alloy annealed at 1300 °C for 15 days. The light grey phase was λ_3 and the dark grey phase was (αCo). The two-phase microstructure of the λ_2 phase (dark grey) and μ-Co_6Ta_7 phase (light grey) was identified in the $Co_{60}Re_1Ta_{39}$ alloy annealed at 1300 °C for 15 days, as shown in Figure 2j. The corresponding XRD pattern is displayed in Figure 3d.

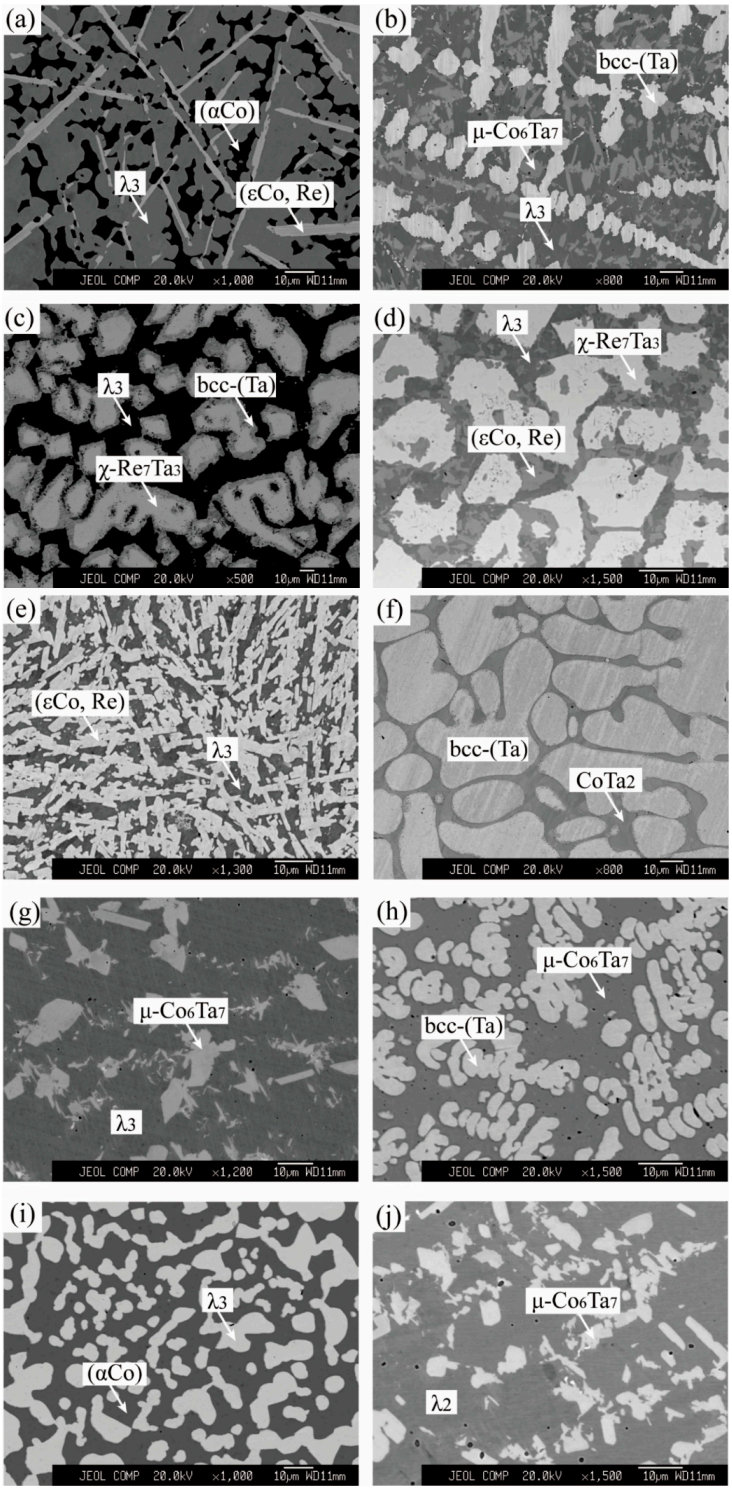

Figure 2. Back-scattered electron (BSE) images of the typical ternary Co-Re-Ta alloys: (**a**) The $Co_{74}Re_{16}Ta_{10}$ alloy annealed at 1100 °C for 50 days; (**b**) the $Co_{44}Re_{14}Ta_{42}$ alloy annealed at 1200 °C for 35 days; (**c**) the $Co_{31}Re_{35}Ta_{34}$ alloy annealed at 1300 °C for 25 days; (**d**) the $Co_{45}Re_{30}Ta_{25}$ alloy annealed at 1300 °C for 25 days; (**e**) the $Co_{54}Re_{25}Ta_{21}$ alloy annealed at 1100 °C for 65 days; (**f**) the $Co_{22}Re_5Ta_{73}$ alloy annealed at 1100 °C for 50 days; (**g**) the $Co_{58}Re_3Ta_{39}$ alloy annealed at 1200 °C for 35 days; (**h**) the $Co_{25}Re_{20}Ta_{55}$ alloy annealed at 1200 °C for 50 days; (**i**) the $Co_{80}Re_{11}Ta_9$ alloy annealed at 1300 °C for 15 days; (**j**) the $Co_{60}Re_1Ta_{39}$ alloy annealed at 1300 °C for 15 days.

In order to figure out the phase boundary between the λ_3 and λ_2 phases, several alloys were prepared. Unfortunately, all the compositions were located at single field region, which meant that the λ_2/λ_3 two-phase field was extremely narrow. This was consistent with that of the Co-Ta binary. The phase boundaries were then plotted with approximations based on the microstructure observation results of these single-phased compositions. Figure 4a,b shows the typical XRD patterns of the $Co_{66}Re_5Ta_{29}$ and $Co_{68}Re_3Ta_{29}$ alloys annealed at 1300 °C for 15 days, which were confirmed to be λ_3 and λ_2 single phases, respectively. The corresponding microstructure was consistent with the results.

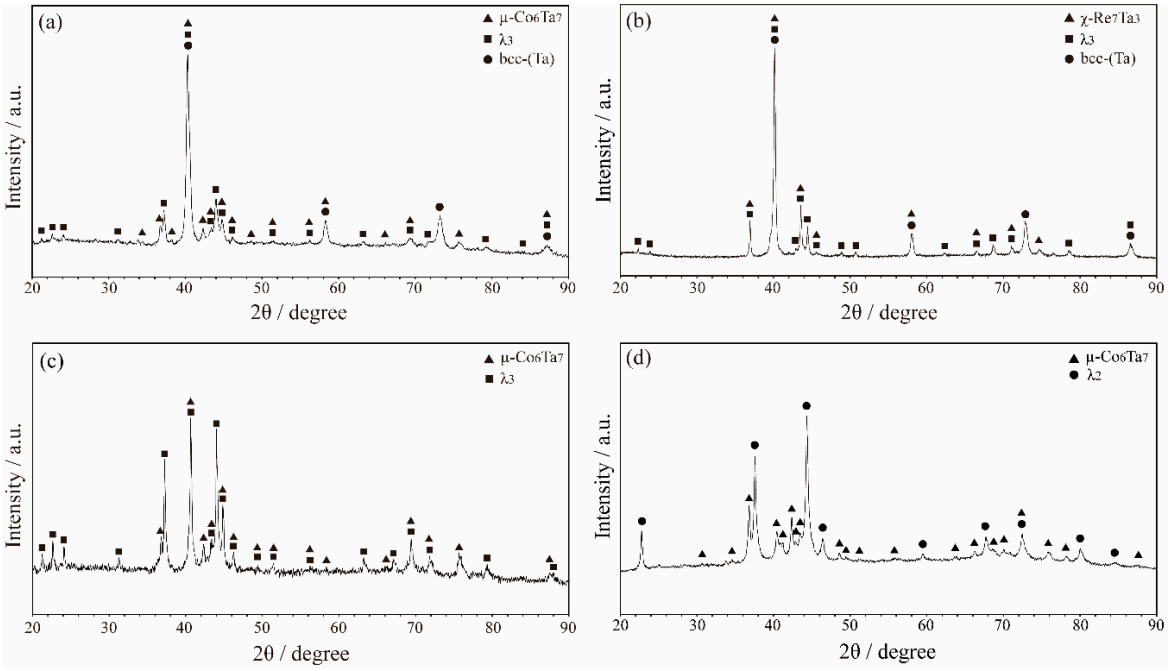

Figure 3. X-ray diffraction patterns obtained from (**a**) the $Co_{44}Re_{14}Ta_{42}$ alloy annealed at 1200 °C for 35 days, (**b**) the $Co_{31}Re_{35}Ta_{34}$ alloy annealed at 1300 °C for 25 days, (**c**) the $Co_{58}Re_3Ta_{39}$ alloy annealed at 1200 °C for 35 days, and (**d**) the $Co_{60}Re_1Ta_{39}$ alloy annealed at 1300 °C for 15 days.

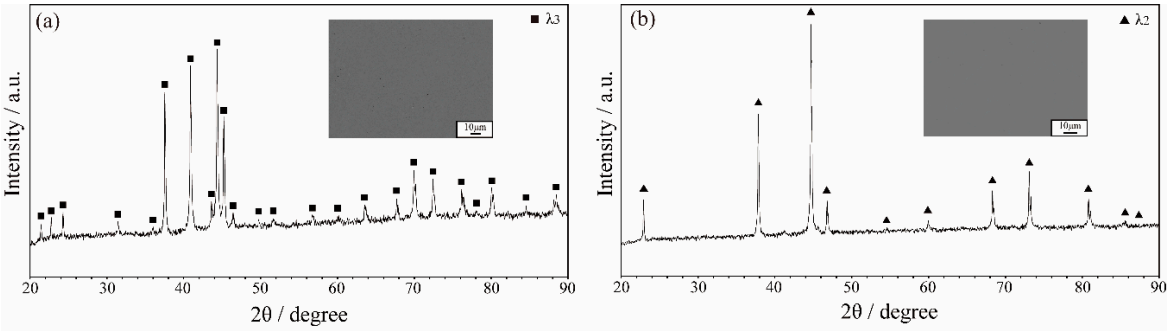

Figure 4. X-ray diffraction patterns obtained from (**a**) the $Co_{66}Re_5Ta_{29}$ alloy annealed at 1200 °C for 35 days and (**b**) the $Co_{68}Re_3Ta_{29}$ alloy annealed at 1300 °C for 15 days.

3.2. Isothermal Sections

All the equilibrium compositions of the Co-Re-Ta ternary system at 1100, 1200, and 1300 °C are listed in Tables 2–4, respectively. Figure 5a–c shows the isothermal sections at 1100, 1200, and 1300 °C based on the experimental data, respectively. The λ_2 single phase, λ_3 single phase, two-phase equilibrium, and three-phase equilibrium are characterized by different symbols. The solid triangle represents the determined three-phase equilibrium while the dashed triangle represents the undetermined three-phase equilibrium.

Table 2. Equilibrium compositions of the Co-Re-Ta ternary system at 1100 °C as determined in the present work.

Nominal Alloys (at. %)	Annealed Time (days)	Phase Equilibrium	Composition (at. %)					
		Phase 1/Phase 2/Phase 3	Phase 1		Phase 2		Phase 3	
			Re	Ta	Re	Ta	Re	Ta
$Co_{31}Re_{35}Ta_{34}$	65	λ_3/bcc-(Ta)/χ-Re_7Ta_3	19.7	26.5	46.5	45.5	52.7	34.8
$Co_{45}Re_{30}Ta_{25}$	65	λ_3/(εCo, Re)/χ-Re_7Ta_3	20.1	25.5	30.4	22.0	60.1	26.0
$Co_{60}Re_{20}Ta_{20}$	65	(εCo, Re)/λ_3	27.3	16.6	16.5	20.5		
$Co_{45}Re_{20}Ta_{35}$	65	bcc-(Ta)/λ_3	41.4	48.4	13.1	30.9		
$Co_{25}Re_{20}Ta_{55}$	65	μ-Co_6Ta_7/bcc-(Ta)	2.3	50.6	34.1	58.3		
$Co_{54}Re_{25}Ta_{21}$	65	(εCo, Re)/λ_3	28.7	19.1	18.4	22.9		
$Co_{78}Re_5Ta_{17}$	50	(αCo)/λ_3	2.7	3.3	4.7	21.8		
$Co_{44}Re_{14}Ta_{42}$	50	λ_3/μ-Co_6Ta_7/bcc-(Ta)	2.7	33.8	3.8	43.7	39.2	51.2
$Co_{22}Re_5Ta_{73}$	50	$CoTa_2$/bcc-(Ta)	0.7	65.8	8.9	87.5		
$Co_{58}Re_3Ta_{39}$	50	λ_3/μ-Co_6Ta_7	1.9	33.6	3.2	43.4		
$Co_{80}Re_2Ta_{18}$	50	(αCo)/λ_3	0.9	3.5	1.8	22.7		
$Co_{80}Re_5Ta_{15}$	50	(αCo)/λ_3	3.5	3.6	5.7	20.8		
$Co_{80}Re_{11}Ta_9$	50	(αCo)/λ_3	9.2	2.7	13.8	17.2		
$Co_{74}Re_{16}Ta_{10}$	50	(αCo)/λ_3/(εCo, Re)	10.1	2.4	15.2	17.3	25.0	14.2
$Co_{54}Re_{18}Ta_{28}$	50	λ_3	18.2	28.3				
$Co_{89}Re_5Ta_6$	50	(αCo)/λ_3	4.6	3.7	7.5	19.6		
$Co_{33}Re_5Ta_{62}$	50	$CoTa_2$/bcc-(Ta)	1.7	59.2	18.0	77.3		
$Co_{30}Re_{10}Ta_{60}$	50	μ-Co_6Ta_7/bcc-(Ta)	1.7	54.2	24.0	71.3		
$Co_{69}Re_9Ta_{22}$	50	λ_3	9.3	22.3				
$Co_{70}Re_5Ta_{25}$	50	λ_3	4.5	24.9				
$Co_{71}Re_1Ta_{28}$	50	λ_2	0.8	28.2				
$Co_{68}Re_3Ta_{29}$	50	λ_2	2.7	28.7				
$Co_{66}Re_5Ta_{29}$	50	λ_3	4.7	28.5				
$Co_{64}Re_7Ta_{29}$	50	λ_3	7.3	28.9				
$Co_{60}Re_1Ta_{39}$	50	λ_2/μ-Co_6Ta_7	0.7	32.3	1.2	43.7		
$Co_{28}Re_6Ta_{66}$	50	$CoTa_2$/bcc-(Ta)	1.4	60.2	14.2	80.7		
$Co_{43}Re_1Ta_{56}$	50	$CoTa_2$/μ-Co_6Ta_7	0.9	57.8	1.1	54.8		

Table 3. Equilibrium compositions of the Co-Re-Ta ternary system at 1200 °C as determined in the present work.

Nominal Alloys (at. %)	Annealed Time (days)	Phase Equilibrium	Composition (at. %)					
		Phase 1/Phase 2/Phase 3	Phase 1		Phase 2		Phase 3	
			Re	Ta	Re	Ta	Re	Ta
$Co_{31}Re_{35}Ta_{34}$	50	λ_3/bcc-(Ta)/χ-Re_7Ta_3	21.7	26.1	50.0	47.6	56.6	31.4
$Co_{45}Re_{30}Ta_{25}$	50	λ_3/(εCo, Re)/χ-Re_7Ta_3	21.7	25.4	31.3	24.3	59.9	26.8
$Co_{60}Re_{20}Ta_{20}$	50	(εCo, Re)/λ_3	27.2	18.7	17.2	20.9		
$Co_{45}Re_{20}Ta_{35}$	50	bcc-(Ta)/λ_3	41.1	48.6	14.0	31.9		
$Co_{25}Re_{20}Ta_{55}$	50	μ-Co_6Ta_7/bcc-(Ta)	2.8	51.1	35.3	58.7		
$Co_{54}Re_{25}Ta_{21}$	50	(εCo, Re)/λ_3	28.0	20.9	20.1	22.9		
$Co_{78}Re_5Ta_{17}$	35	(αCo)/λ_3	2.7	4.4	4.3	21.9		
$Co_{44}Re_{14}Ta_{42}$	35	λ_3/μ-Co_6Ta_7/bcc-(Ta)	3.5	35.3	4.0	44.2	39.4	50.4
$Co_{22}Re_5Ta_{73}$	35	$CoTa_2$/bcc-(Ta)	0.8	65.2	8.9	86.5		
$Co_{58}Re_3Ta_{39}$	35	λ_3/μ-Co_6Ta_7	2.4	34.4	3.3	43.9		
$Co_{80}Re_2Ta_{18}$	35	(αCo)/λ_3	1.4	4.9	1.8	22.5		
$Co_{80}Re_5Ta_{15}$	35	(αCo)/λ_3	3.2	4.2	5.5	21.1		
$Co_{80}Re_{11}Ta_9$	35	(αCo)/λ_3	9.7	3.0	13.6	18.4		
$Co_{74}Re_{16}Ta_{10}$	35	(αCo)/λ_3/(εCo, Re)	11.2	2.8	15.5	17.6	24.9	15.3
$Co_{54}Re_{18}Ta_{28}$	35	λ_3	18.3	28.2				
$Co_{89}Re_5Ta_6$	35	(αCo)/λ_3	4.3	4.5	7.1	20.6		
$Co_{33}Re_5Ta_{62}$	35	$CoTa_2$/bcc-(Ta)	1.5	59.6	19.5	76.8		
$Co_{30}Re_{10}Ta_{60}$	35	μ-Co_6Ta_7/bcc-(Ta)	2.0	55.1	23.5	72.2		
$Co_{69}Re_9Ta_{22}$	35	λ_3	8.4	22.0				
$Co_{70}Re_5Ta_{25}$	35	λ_3	4.5	24.8				
$Co_{71}Re_1Ta_{28}$	35	λ_2	0.8	28.0				
$Co_{68}Re_3Ta_{29}$	35	λ_2	2.6	28.8				
$Co_{66}Re_5Ta_{29}$	35	λ_3	4.8	29.0				
$Co_{64}Re_7Ta_{29}$	35	λ_3	7.0	28.8				
$Co_{60}Re_1Ta_{39}$	35	λ_2/μ-Co_6Ta_7	0.5	32.4	1.0	44.1		
$Co_{28}Re_6Ta_{66}$	35	$CoTa_2$/bcc-(Ta)	1.3	60.2	15.9	79.6		
$Co_{43}Re_1Ta_{56}$	35	$CoTa_2$/μ-Co_6Ta_7	0.6	60.5	1.3	54.8		

Table 4. Equilibrium compositions of the Co-Re-Ta ternary system at 1300 °C as determined in the present work.

Nominal Alloys (at. %)	Annealed Time (days)	Phase Equilibrium	Composition (at. %)					
		Phase 1/Phase 2/Phase 3	Phase 1		Phase 2		Phase 3	
			Re	Ta	Re	Ta	Re	Ta
$Co_{31}Re_{35}Ta_{34}$	25	λ_3/bcc-(Ta)/χ-Re_7Ta_3	22.2	27.1	49.0	48.5	56.6	32.6
$Co_{45}Re_{30}Ta_{25}$	25	λ_3/(εCo, Re)/χ-Re_7Ta_3	22.6	26.1	32.0	23.2	58.7	25.8
$Co_{60}Re_{20}Ta_{20}$	25	(εCo, Re)/λ_3	27.5	17.0	17.3	20.6		
$Co_{45}Re_{20}Ta_{35}$	25	bcc-(Ta)/λ_3	42.8	48.9	14.2	32.8		
$Co_{25}Re_{20}Ta_{55}$	25	μ-Co_6Ta_7/bcc-(Ta)	3.9	51.2	35.5	58.9		
$Co_{54}Re_{25}Ta_{21}$	25	(εCo, Re)/λ_3	28.8	18.9	19.7	22.1		
$Co_{78}Re_5Ta_{17}$	15	(αCo)/λ_3	2.8	5.5	5.0	21.3		
$Co_{44}Re_{14}Ta_{42}$	15	λ_3/μ-Co_6Ta_7/bcc-(Ta)	5.5	36.4	6.1	43.2	41.8	50.4
$Co_{22}Re_5Ta_{73}$	15	$CoTa_2$/bcc-(Ta)	0.8	65.2	8.7	87.6		
$Co_{58}Re_3Ta_{39}$	15	λ_3/μ-Co_6Ta_7	2.7	35.4	3.6	44.0		
$Co_{80}Re_2Ta_{18}$	15	(αCo)/λ_3	1.3	5.6	1.9	22.3		
$Co_{80}Re_5Ta_{15}$	15	(αCo)/λ_3	3.5	5.0	5.9	20.8		
$Co_{80}Re_{11}Ta_9$	15	(αCo)/λ_3	10.0	3.8	13.8	17.8		
$Co_{74}Re_{16}Ta_{10}$	15	(αCo)/λ_3/(εCo, Re)	13.0	2.6	16.2	17.8	26.0	14.2
$Co_{54}Re_{18}Ta_{28}$	15	λ_3	18.2	28.5				
$Co_{89}Re_5Ta_6$	15	(αCo)/λ_3	4.8	5.0	7.2	22.4		
$Co_{33}Re_5Ta_{62}$	15	$CoTa_2$/bcc-(Ta)	2.1	59.2	19.2	76.2		
$Co_{30}Re_{10}Ta_{60}$	15	μ-Co_6Ta_7/bcc-(Ta)	2.4	54.1	24.2	71.4		
$Co_{69}Re_9Ta_{22}$	15	λ_3	8.9	22.0				
$Co_{70}Re_5Ta_{25}$	15	λ_3	4.5	24.5				
$Co_{71}Re_1Ta_{28}$	15	λ_2	0.7	27.8				
$Co_{68}Re_3Ta_{29}$	15	λ_2	2.7	28.6				
$Co_{66}Re_5Ta_{29}$	15	λ_3	4.6	28.4				
$Co_{64}Re_7Ta_{29}$	15	λ_3	7.0	28.6				
$Co_{60}Re_1Ta_{39}$	15	λ_2/μ-Co_6Ta_7	0.8	32.3	1.3	44.2		
$Co_{28}Re_6Ta_{66}$	15	$CoTa_2$/bcc-(Ta)	1.8	58.3	14.9	81.1		
$Co_{43}Re_1Ta_{56}$	15	$CoTa_2$/μ-Co_6Ta_7	0.6	59.7	1.3	54.9		

Figure 5a shows the 1100 °C isothermal section of the Co-Re-Ta ternary system. There were three solid solution phases of (αCo), (εCo, Re), and bcc-(Ta), two Laves phases of λ_2 and λ_3, and the intermetallic compounds of the μ-Co_6Ta_7, $CoTa_2$, and χ-Re_7Ta_3 phases. Investigations of the $Co_{74}Re_{16}Ta_{10}$, $Co_{44}Re_{14}Ta_{42}$, $Co_{31}Re_{35}Ta_{34}$, and $Co_{45}Re_{30}Ta_{25}$ alloys were used to determine the three-phase equilibria of (αCo) + (εCo, Re) + λ_3, λ_3 + bcc-(Ta) + μ-Co_6Ta_7, λ_3 + χ-Re_7Ta_3 + bcc-(Ta), and (εCo, Re) + λ_3 + χ-Re_7Ta_3, respectively. Seven alloys were confirmed to be single phases, two alloys ($Co_{71}Re_1Ta_{28}$ and $Co_{68}Re_3Ta_{29}$) were located in the λ_2 single-phase region, and five alloys ($Co_{54}Re_{18}Ta_{28}$, $Co_{69}Re_9Ta_{22}$, $Co_{70}Re_5Ta_{25}$, $Co_{66}Re_5Ta_{29}$ and $Co_{64}Re_7Ta_{29}$) were located in the λ_3 single-phase region. The solubility of Re in the λ_3 phase was measured to be about 20.1 at. % while the solubility of Re in the λ_2 phase was measured to be about 3.8 at. %. The λ_3 phase extended from the left side to the right side of the λ_2 phase and was wrapped around the λ_2 phase. The solubility of Re in the μ-Co_6Ta_7 and $CoTa_2$ phases was quite small at roughly 3.3 at. % and 1.5 at. %, respectively. The solubility of Co in the χ-Re_7Ta_3 phase was about 16.8 at. %. The (εCo, Re) phase extended from the Re-rich side to the Co-rich side, and the solubility of Ta in (εCo, Re) phase was about 21.7 at. %.

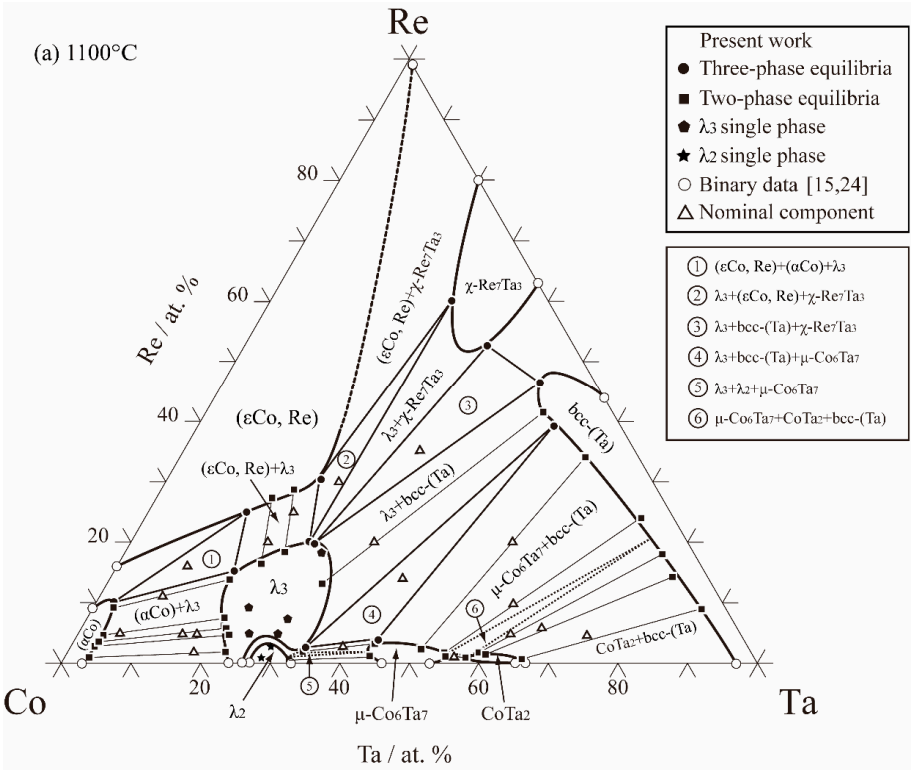

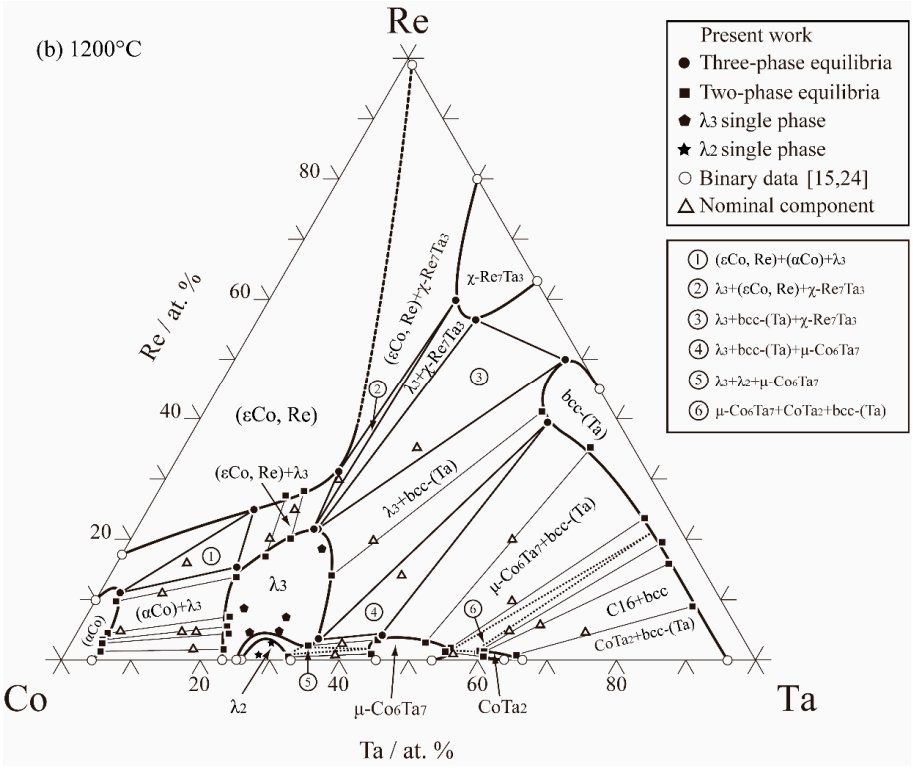

Figure 5. *Cont.*

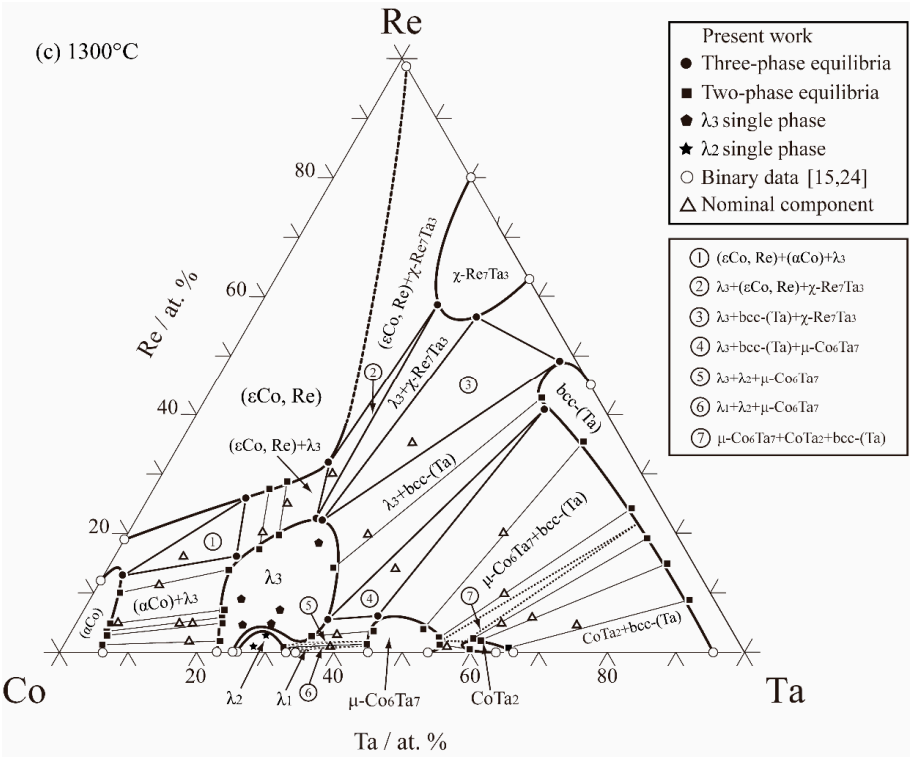

Figure 5. Experimentally determined isothermal section of the Co-Re-Ta system: (**a**) 1100 °C, (**b**) 1200 °C, (**c**) 1300 °C.

Figure 5b shows the isothermal section at 1200 °C. Four three-phase regions of the (αCo) + (εCo, Re) + λ_3, λ_3 + bcc-(Ta) + μ-Co_6Ta_7, λ_3 + χ-Re_7Ta_3 + bcc-(Ta), and (εCo, Re) + λ_3 + χ-Re_7Ta_3 were experimentally determined. The 1200 °C isothermal section was similar to the 1100 °C isothermal section. The solubility of Re in the λ_3 phase increased a little from 20.1 at. % at 1100 °C to 21.5 at. % at 1200 °C. The solubility of Re in the λ_2 phase was about 3.5 at. %, almost the same as at 1100 °C. The μ-Co_6Ta_7 and $CoTa_2$ phases dissolved about 3.8 at. % and 1.4 at. % Re, respectively. The solubility of Ta in the (εCo, Re) phase was about 24.1 at. %. The solubility of Co in the χ-Re_7Ta_3 phase was measured to decrease from 16.8 at. % to 13.4 at. %. The three-phase region of λ_3 + χ-Re_7Ta_3 + bcc-(Ta) at the 1200 °C isothermal section was larger than that of the 1100 °C isothermal section, while the (εCo, Re) + λ_3 + χ-Re_7Ta_3 three-phase region was smaller.

The isothermal section at 1300 °C is shown in Figure 5c. Compared to the 1200 and 1300 °C isothermal sections, another Laves phase of λ_1, which existed at 1293 °C~1587 °C in the Co-Ta binary system, appeared in the 1100 °C isothermal section. However, the solubility of Re was so small that it was not identified. The 1300 °C isothermal section had one more three-phase region (λ_1 + λ_2 + μ-Co_6Ta_7) than in the 1100 and 1200 °C isothermal sections. The solubility of Re in the λ_3 and λ_2 phases was about 22.3 at. %, 3.6 at. %, respectively. The solubility of Re in μ-Co_6Ta_7 was found to be about 6.1 at. %, occupying the most out of all the investigated isothermal sections. The $CoTa_2$ phase dissolved about 1.8 at. % Re. The solubility of Ta in the (εCo, Re) phase was about 23.2 at. %. There were seven three-phase regions of (αCo) + (εCo, Re) + λ_3, λ_3 + bcc-(Ta) + μ-Co_6Ta_7, λ_3 + χ-Re_7Ta_3 + bcc-(Ta), (εCo, Re) + λ_3 + χ-Re_7Ta_3, λ_3 + λ_2 + μ-Co_6Ta_7, λ_1 + λ_2 + μ-Co_6Ta_7, and $CoTa_2$ + μ-Co_6Ta_7 + bcc-(Ta) existing at 1300 °C. The former four three-phase regions were experimentally confirmed, and the last three three-phase regions were not experimentally evidenced. The three-phase equilibrium of λ_3 + bcc-(Ta) + μ-Co_6Ta_7 was smaller than those in the 1100 and 1200 °C isothermal sections.

4. Conclusions

The isothermal sections of the Co-Re-Ta ternary system at 1100, 1200, and 1300 °C were experimentally investigated. The results were as follows: (1) There were six three-phase regions at the 1100 and 1200 °C isothermal sections and seven three-phase regions at the 1300 °C isothermal section; (2) the (εCo, Re) phase had a large solubility of Ta and extended from the Re-rich side to the Co-rich side; (3) the λ_3 phase, with a large solubility of Re, surrounded the λ_2 phase which dissolved a little Re; (4) the solubility of Re in the $CoTa_2$ phase changed little while the solubility of Re in the μ-Co_6Ta_7 phase increased with the temperature increase from 1100 to 1300 °C; (5) no ternary compound was found.

Author Contributions: Conceptualization, X.L. and C.W.; funding acquisition, X.L. and C.W.; investigation, D.W., J.Z. (Jinbin Zhang), J.H. and Y.L.; supervision, X.L. and C.W.; writing—original draft, D.W.; writing—review and editing, M.Y., J.Z. (Jiahua Zhu), L.L., Y.C. and S.Y.

Funding: This work was supported by the National Key R&D Program of China (Grant No. 2016YFB0701401) and National Natural Science Foundation of China (Grant Nos. 51831007 and 51471138).

Acknowledgments: This work was supported by the National Key R&D Program of China (Grant No. 2016YFB0701401) and National Natural Science Foundation of China (Grant Nos. 51831007 and 51471138).

Conflicts of Interest: The authors declare no conflicts of interest.

References

1. Sato, J.; Omori, T.; Oikawa, K.; Ohnuma, I.; Kainuma, R.; Ishida, K. Cobalt-base high-temperature alloys. *Science* **2006**, *312*, 90–91. [CrossRef] [PubMed]
2. Liu, E.; Guan, X.; Zheng, Z. Effect of rhenium on solidification and segregation of nickel-based superalloy. *Rare Met.* **2011**, *30*, 320–322. [CrossRef]
3. Blavette, D.; Caron, P.; Khan, T. An atom probe investigation of the role of rhenium additions in improving creep resistance of Ni-base superalloys. *Scr. Metall.* **1986**, *20*, 1395–1400. [CrossRef]
4. Preußner, J.; Rudnik, Y.; Brehm, H.; Völkl, R.; Glatzel, U. A dislocation density based material model to simulate the anisotropic creep behavior of single-phase and two-phase single crystals. *Int. J. Plasticity* **2009**, *25*, 973–994. [CrossRef]
5. Huang, M.; Zhu, J. An overview of rhenium effect in single-crystal superalloys. *Rare Met.* **2016**, *35*, 127–139. [CrossRef]
6. Shang, L.; Cai, Q.; Liu, C.; Qi, L. Effects of Re doping on properties of Co-based alloy coating treated by laser cladding. *Rare Met.* **2002**, *26*, 173–178.
7. Cardonne, S.M.; Kumar, P.; Michaluk, C.A.; Schwartz, H.D. Tantalum and its alloys. *Int. J. Refract. Met. Hard Mater.* **1995**, *13*, 187–194. [CrossRef]
8. Zheng, L.; Zhang, G.; Lee, T.L.; Gorley, M.J.; Wang, Y.; Xiao, C.; Li, Z. The effects of Ta on the stress rupture properties and microstructural stability of a novel Ni-base superalloy for land-based high temperature applications. *Mater. Des.* **2014**, *61*, 61–69. [CrossRef]
9. Seiser, B.; Drautz, R.; Pettifor, D.G. TCP phase predictions in Ni-based superalloys: Structure maps revisited. *Acta Mater.* **2011**, *59*, 749–763. [CrossRef]
10. Rae, C.M.F.; Reed, R.C. The precipitation of topologically close-packed phases in rhenium-containing superalloys. *Acta Mater.* **2001**, *49*, 4113–4125. [CrossRef]
11. Pessah-Simonetti, M.; Donnadieu, P.; Caron, P.T.C.P. Phase particles embedded in a superalloy matrix: Interpretation and prediction of the orientation relationships. *Scr. Metall. Mater.* **1994**, *30*, 1553–1558. [CrossRef]
12. Elliott, R.P. Constitution of binary alloys First supplement. *J. Less-Common Met.* **1966**, 371–372.
13. Predel, B. Co-Re (Cobalt-Rhenium). In *Ca-Cd-Co-Zr*; Madelung, O., Ed.; SpringerMaterials; Springer: Berlin, Germany, 1993; Volume 5C, pp. 1–3.
14. Liu, X.J.; Lin, J.Y.; Lu, Y.; Guo, Y.H.; Wang, C.P. Assessment of the atomic mobility for the fcc phase of Ni–Co–X (X = Re and Ru) system. *Calphad* **2014**, *45*, 138–144. [CrossRef]
15. Guo, C.; Wu, T.; Li, C.; Du, Z. Thermodynamic re-assessment of the Re–X (X = Al, Co, Cr, Ta) binary systems. *Calphad* **2018**, *61*, 33–40. [CrossRef]

16. Greenfield, P.; Beck, P.A. Intermediate phases in binary systems of certain transition elements. *JOM* **1956**, *8*, 265–276. [CrossRef]
17. Cui, Y.; Jin, Z. Assessment of the Re–Ta binary system. *J. Alloys Compd.* **1999**, *285*, 150–155. [CrossRef]
18. Liu, Z.K.; Chang, Y.A. Evaluation of the thermodynamic properties of the Re–Ta and Re–W systems. *J. Alloys Compd.* **2000**, *299*, 153–162. [CrossRef]
19. Itoh, H.; Aoki, Y.; Nakamichi, T.; Yamamoto, M. Crystal structures, homogeneity ranges and magnetic properties of tantalum-cobalt Laves phases. *Z. Metallk.* **1974**, *65*, 149.
20. Okamoto, H. Co-Ta (Cobalt-Tantalum). *J. Phase Equilib. Diffus.* **2004**, *25*, 571–572. [CrossRef]
21. Liu, Z.K.; Chang, Y.A. Thermodynamic assessment of the Co-Ta system. *Calphad* **1999**, *23*, 339–356. [CrossRef]
22. Kaufman, L. Coupled thermochemical and phase diagram data for tantalum based binary alloys. *Calphad* **1991**, *15*, 243–259. [CrossRef]
23. Ponsioen, J.; Van Vucht, J. The Structure of β-$TaCo_3$ and the effect of the substitution of Ta and Co by related elements. *Philipp. Res. Rep.* **1967**, *22*, 161–169.
24. Shinagawa, K.; Chinen, H.; Omori, T.; Oikawa, K.; Ohnuma, I.; Ishida, K.; Kainuma, R. Phase equilibria and thermodynamic calculation of the Co–Ta binary system. *Intermetallics* **2014**, *49*, 87–97. [CrossRef]